ingegneria sismica
International Journal of Earthquake Engineering
Anno XLIII - Num. 3 - 2026

Study on the Law of Lip-shaped Multiple Cracks Propagation Coalescence in Brittle Materials

Tianzhu Liu[1,*], *Hong Zhang*[1], *Xuelan Hu*[1], *Xiangping Li*[1] *and Yu Feng*[1]

[1] Sino-European Institute of Aviation Engineering of Civil Aviation University of China Tianjin 300300, Tianjin, China

SUMMARY: *The macroscopic failure of brittle materials normally originates from the unstable propagation of one or multiple dominant cracks, which evolve through the coalescence of distributed internal microcracks and defects. This study focuses on common defects containing both tip and curved-segment features, abstracted as lip-shaped cracks, and establishes corresponding failure criterion. A periodically distributed lip-shaped multiple crack model was developed to investigate three critical factors affecting crack interactions: crack inclination angle, crack width-to-length ratio, and crack spacing, by which four coalescence patterns were predicted. Validation was conducted via coalescence simulation and comparation with literatures' experiments. The coalescence mechanisms and impact on performance of lip-shaped multiple cracks were ultimately revealed. The principal conclusions are summarized as follows: (1) Four coalescence patterns of lip-shaped multiple cracks were summarized, thereinto the most common coalescence pattern is the coalescence between tip and abdomen. The coalescence pattern is most sensitive to the change of crack inclination angle;(2) Compared with the experimental results, this study successfully simulates the complex coalescences in brittle materials; (3) The crack inclination angle and spacing of lip-shaped cracks have a significant impact on the performance of the model: the smaller the crack inclination angle, the smaller the tensile strength and the greater the stiffness of the model; the smaller the crack spacing, the smaller the model failure displacement.*

KEYWORDS: *lip-shaped crack; crack propagation; brittle materials; coalescence law*

1 Introduction

The macroscopic failure of brittle materials normally originates from the unstable propagation of one or multiple dominant cracks, which evolve through the coalescence of distributed internal microcracks and defects [1]. During loading and crack propagation, the coupling of stress fields between these defects (e.g., cracks or voids) influences the local stress distribution near individual cracks, thereby influencing the direction and path of dominant crack propagation. However, crack propagation in brittle materials during failure—whether involving linear cracks or elliptical voids—exhibits inherent complexity. The study of crack propagation serves as the foundation for understanding void-related failure mechanisms, as both cracks and voids induce brittle material fracture through stress concentration, a critical distinction lies in the geometric sharpness: the stress concentration at void peripheries is significantly less pronounced than that at crack tips [2]. In practical application, defects combining both tip and curved-segment features (e.g., cracks with multiple curvatures or voids with irregular

*2022122021@cauc.edu.cn
https://doi.org/10.65102/is20261113
Published: 10 June, 2026

geometries) frequently coexist. **Figure 1** shows a micrograph of carburized 1215 steel containing "lip-shaped-crack-like" defects. This paper abstracts such hybrid defects as lip-shaped cracks characterized by both tip and curved-segment attributes. Compared to linear cracks (with pure tip features) or elliptical voids (with pure curvature), lip-shaped cracks better represent realistic defect morphologies and are more practical.

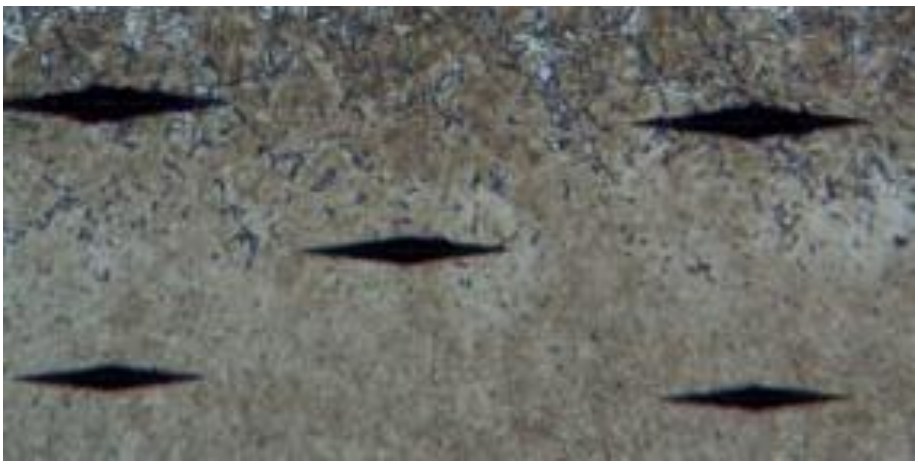

Figure 1: The micrograph of carburized 1215 steel containing "lip-shaped-crack-like" defects (Courtesy of Metal test Inc. and CES Engineering Guide.)

Reference [3] demonstrated that strongly perturbed cracks in brittle materials deflect due to interactions with sparsely implanted defects. Reference [4] revealed that cracks kink toward nearby square voids, with the kinking amplitude increasing as the void-crack distance decreases. Reference [5] employing distributed dislocation methods, found that microcracks significantly change the stress field and propagation path of dominant cracks through stress concentration effects. Reference [6] uncovered mutual attraction and coalescence patterns among multiple cracks based on their relative positions. However, these studies did not figure out how tip or curved-segment features influence crack propagation paths or account for complex coalescence situations. Reference [7] proposed three coalescence strategies for multiple crack systems in brittle rocks, successfully simulating complex crack growth and linkage, yet neglecting the role of crack parameters. Reference [8] investigated the effects of crack width on edge crack initiation and propagation. Reference [9] analyzed the influence of periodically distributed linear cracks' density and inclination angle on coalescence and strength. Reference [10] identified seven fundamental crack coalescence patterns and observed ten coalescence patterns under biaxial compression. Nevertheless, these works overlooked cracks with curved-segment characteristics. Reference [11] derived stress intensity factors and maximum energy release rates for I-II mixed mode lip-shaped cracks using conformal mapping and complex variable methods but did not explore multiple crack coalescence in brittle materials.

In summary, this study addresses common defects featuring both tip and curved-segment characteristics by abstracting them as lip-shaped cracks and establishing a corresponding lip-shaped crack failure criterion. Through the periodically distributed lip-shaped multiple cracks model, the interactions among cracks were systematically investigated by analyzing three critical parameters: crack inclination angle(γ), width-to-length ratio(β), and spacing(s), predicting four distinct coalescence patterns. These predictions were validated via crack propagation simulations and comparation with literatures' experiment. The coalescence mechanisms and impact on performance of lip-shaped multiple cracks in brittle materials were ultimately revealed.

2 Research on the failure criterion of lip-shaped crack propagation

The proposed I-II mixed mode lip-shaped crack propagation model is schematically illustrated in **Figure 2**. A lip-shaped crack with half-length a, half-width h, and width-length ratio β=h/a, is embedded in an infinite plane subjected to far-field uniaxial tensile loading σ_y^{∞}. Three coordinate systems are defined: the global coordinate system (O, x, y) with its origin at the crack center O, the local coordinate system (O′, x′, y′) aligned with the crack's major axis, and the tip-local coordinate system (O″, x″, y″) originating at the crack tip O″ with the x″-axis extending along the major axis. The inclination angle γ quantifies the angular deviation between the crack's major axis and the global x-axis, while the local cracking angle θ characterizes the crack-tip path under off-axis tensile loading relative to the major axis.

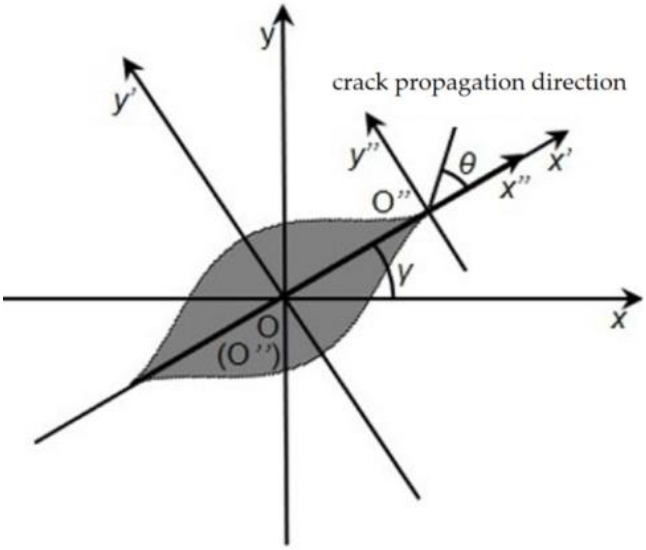

Figure 2: Schematic diagram of I-II mixed mode lip-shaped crack propagation.

According to literature [12], the expression of the stress intensity factor *K* at the tip of I-II mixed mode lip-shaped crack is as follows:

$$K = \sqrt{\pi a}\,\frac{\sigma^{\infty}}{4(1+m)}\left\{\begin{array}{c}\dfrac{(1+m)^4(1-m)+2\cos(2\gamma)\left[(1+m)^3+\left(1+m^2\right)^2\right]}{(1+m^2)^2}\\ i\,\dfrac{2\sin(2\gamma)(1-m)}{1+m^2}\end{array}\right\} \tag{1}$$

The real part of *K* is the mode I stress intensity factor K_I, and the opposite number of the imaginary part is the expression of the mode II stress intensity factor K_{II} ($K = K_I - i\,K_{II}$).

In this formula, *m* is a parameter that is only related to the width-length ratio of lip-shaped cracks ($\beta = h/a$), and the expression is as follows:

$$m = \frac{\left(\sqrt{1+\beta^2}+\beta-1\right)}{\left(\sqrt{1+\beta^2}+\beta+1\right)} \tag{2}$$

As shown in Figure 2, the propagation of the I-II mixed mode lip-shaped crack does not necessarily extend along the direction of the crack tip ($\theta \neq 0$), but extends along the θ angle direction. According to literature, the energy release rate *G* of the I-II mixed mode lip-shaped

crack can be written as the following formula:

$$G(\theta) = \frac{1-\nu^2}{E}\left(\frac{\pi-\theta}{\pi+\theta}\right)^{\frac{\theta}{\pi}}\left(\frac{2}{3+cos^2\theta}\right)^2\left(K_I^2(1+3\,cos^2\theta) + 4K_I K_{II}\,sin\,2\theta + K_{II}^2(9-5\,cos^2\theta)\right) \tag{3}$$

In the formula, E is the elastic modulus, v is the Poisson's ratio, K_I and K_{II} can be given by formula (1).

This study adopts the maximum energy release rate (MERR) criterion for crack propagation path analysis, as the stress intensity factor (SIF) criterion, while effective in characterizing stress-strain field intensity near crack tips, inadequately addresses directional crack propagation during coalescence processes. This limitation explains why energy-based criteria are widely selected in brittle material fracture studies. Following the Griffith-Irwin theory, crack initiation occurs when the maximum energy release rate G_{max} at the crack tip reaches the critical value G_{IC}, with propagation aligned along the direction of maximum energy release—corresponding to the cracking angle θ_0, defined as the angular deviation between the propagation direction and the global x-axis. The determination of θ_0 is derived by the extremum principle: the cracking angle satisfies conditions:

$$\begin{cases} \frac{dG(\theta)}{d\theta} = 0, \ \theta = \theta_0 \\ \frac{d^2G(\theta)}{d\theta^2} < 0 \end{cases} \tag{4}$$

During the loading of brittle materials containing multiple lip-shaped cracks, stress concentration emerges near individual cracks, where the resultant stress field arises from both inter-crack interactions and external load coupling, leading to deviations in crack propagation direction from the theoretical cracking angle θ_0. This directional inconsistency necessitates combined stress-strain field analysis, as energy release rate (G) and stress intensity factors (K_I,K_{II})—though representing distinct perspectives in linear elastic fracture mechanics (LEFM)—remain mutually consistent for propagation path prediction.

Figure 3 illustrates the variation of θ_0 with crack inclination angle γ, revealing that θ_0 monotonically increases as γ rises from 0°to 75°. For cracks with width-to-length ratio β<0.6, the growth rate of θ_0 diminishes with increasing γ, while at β=0.6, θ_0 exhibits near-linear growth. When β>0.6, characterized by circularized curved segments, θ_0 accelerates sharply with γ. Notably, the lip-shaped crack degenerates into a Griffith-type linear crack at β=0. For $\gamma \in$[0°,50°], larger β values correspond to smaller θ_0 , indicating enhanced Mode I dominance in high- width-length-ratio cracks. However, beyond a critical γ, crack initiation shifts from the tip to the crack abdomen (validated by subsequent simulations) [13, 14], rendering the derived failure criterion inapplicable.

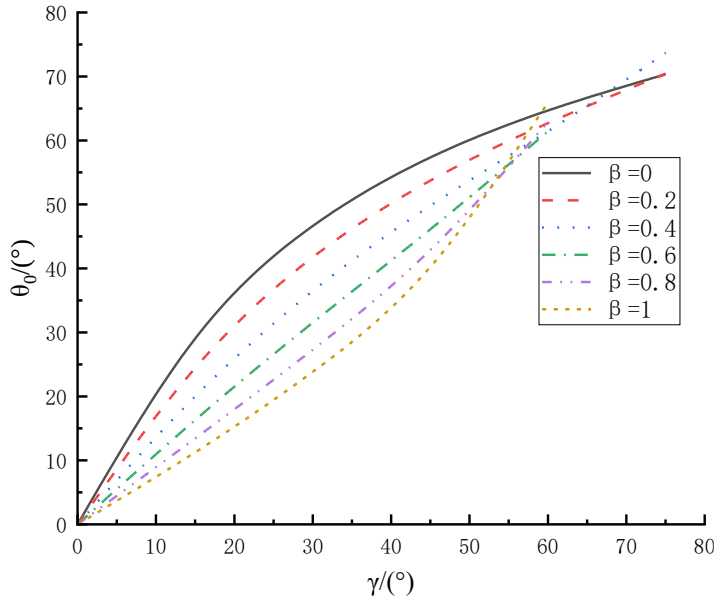

Figure 3: Curve of cracking angle θ_0 for the inclination angles γ variation

Based on Equation (1), the ratio of mode I to mode II stress intensity factors (K_I/K_{II}) was calculated as a function of crack inclination angle γ, as shown in Figure 4, under the geometric parameters a=2 and β=0.4. At γ=0°, K_{II}=0, resulting in a theoretically infinite K_I/K_{II} ratio; hence, **Figure 4** only displays data for $\gamma \in [15°,75°]$. The results demonstrate that K_I/K_{II} decreases monotonically with increasing γ, asymptotically approaching zero. This trend indicates a gradual reduction in normal tensile stress at the crack tip and a corresponding dominance of shear stress under critical propagation conditions, signifying a transition from mode I to mode II fracture dominance at larger inclination angles. Mechanistically, the diminishing K_I/K_{II} ratio reflects enhanced shear-stress-driven crack propagation as γ increases, a critical insight for analyzing directional growth patterns in multi-lip-shaped crack systems.

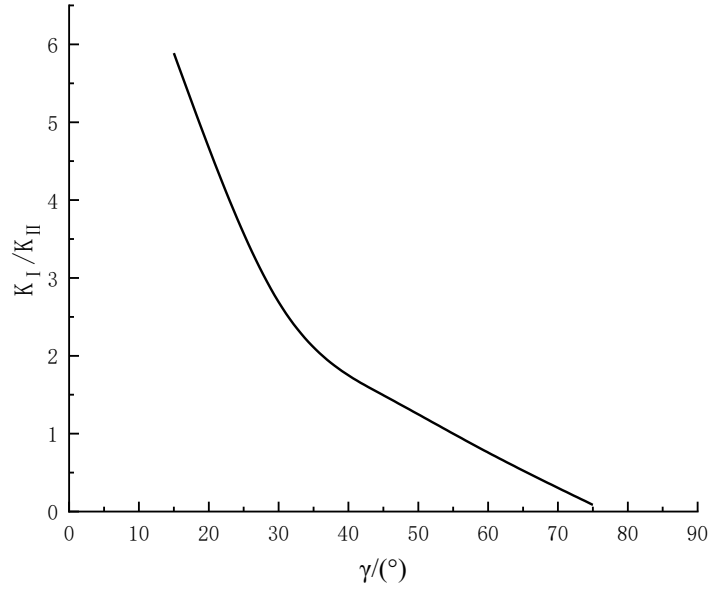

Figure 4: Curve of the stress intensity factor ratio for the inclination angle γ variation ($a = 2mm$, $\beta = 0.4$)

Figure 5 presents the variation of crack tip energy release rate G with width-to-length ratio β for lip-shaped cracks under constant loading (σ=500MPa) and crack half-length (a=0.5mm), across different inclination angles γ. For cracks with γ<5°, G initially increases then decreases with rising β, reflecting a transition from stress intensification to geometric blunting as cracks become more rounded. When γ ranges from 5°to 15°, G exhibits a non-monotonic response, decreasing initially, followed by a local maximum, and subsequently declining with increasing β, suggesting competing effects between shear-tensile coupling and curvature-induced stress redistribution. For γ>15°, G decreases monotonically with β, indicating progressive shear stress dominance and reduced tensile contribution at larger curvatures. Notably, for cracks with $0.3\leq\beta\leq1$, smaller inclination angles ($\gamma\in[0°,35°]$) correlate with lower critical G thresholds, significantly increasing the propensity for unstable propagation.

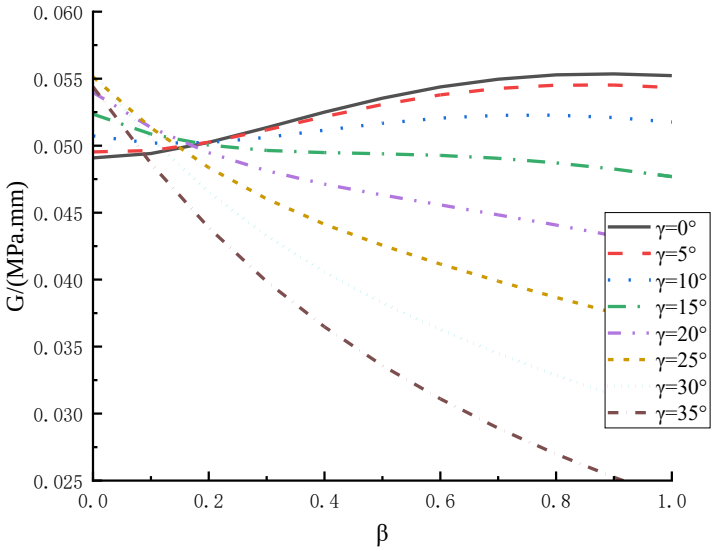

Figure 5: Curve of the energy release rate G for the width-to-length ratio β variation (a = 0.5 mm)

Table 1 and **Figure 6** present a comparative analysis of theoretical and simulated Mode I stress intensity factor (K_I) values at lip-shaped crack tips, along with their percentage discrepancies as functions of inclination angle γ. The results demonstrate close agreement between theoretical predictions and simulation outcomes, with discrepancies consistently below 7% across all tested γ values. This minimal error margin validates the accuracy of the simulation methodology in capturing mixed-mode stress field interactions and geometric nonlinearities inherent to lip-shaped defects.

Table 1: K_I errors for different inclination angles

Inclination angles γ/(°)	Errors/(%)
0	4.491
15	4.396
30	5.306
45	3.224
60	4.380
75	6.061

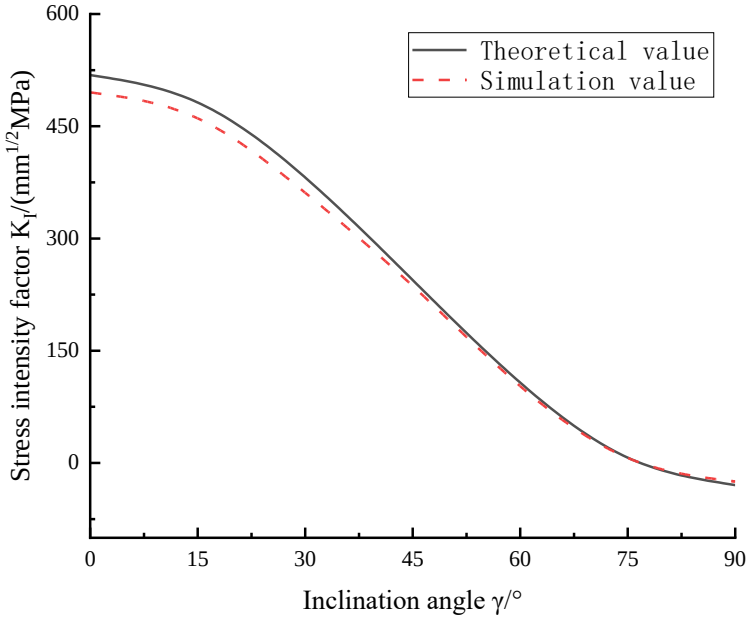

Figure 6: Curve of theoretical and simulated values of K_I for the inclination angle γ variation

3 Stress-strain field analysis near lip-shaped multiple cracks

To investigate stress field interactions among lip-shaped multiple cracks, a periodically distributed lip-shaped multiple crack model was established, with the material selected as ceramic (properties listed in **Table 2**). Numerical simulations were conducted using a bilinear cohesive zone model implemented in ABAQUS.

Table 2: Material properties

Properties	Value
Density /(g/cm^3)	2.5
Young's modulus/(GPa)	300
Poisson ratio	0.25
Tensile strength/(MPa)	1000
Damage energy/(10^{3}N/m)	0.5

Three distinct models—varying in crack inclination angle γ, width-to-length ratio β, and spacing s—were established to investigate stress interactions, with corresponding stress contour plots shown in **Figure 7**, **Figure 8**, and **Figure 9**.

For low inclination angles (γ=0°and 30°), adjacent lip-shaped cracks in the same row exhibit overlapping stress concentration zones near their tips (Figure 7-a), with mutual reinforcement intensifying as γ decreases due to reduced inter-tip distances. As analyzed in Section 2, this configuration is dominated by normal tensile stress on crack surfaces, accompanied by small crack cracking angles θ_0. Further loading under these conditions may trigger tip-to-tip coalescence. With increasing γ, stress concentration shifts toward diagonally adjacent cracks (aligned at 45°, Figure 7-b), while the high-stress region migrates from the tip to the crack abdomen (Figure 7-c). Although crack initiation may still originate from the tip, the reduced normal tensile stress and elevated shear stress result in larger θ_0, with potential crack paths extending from the tip of one crack to the abdomen of another due to geometric misalignment. At γ=90°, stress concentration localizes entirely at crack abdomens (Figure 7-d), eliminating

tip-initiated propagation. Under continued loading, abdominal stress coupling may drive abdomen-to-abdomen coalescence, reflecting a complete transition from tensile-dominated to shear-stress-governed failure mechanisms.

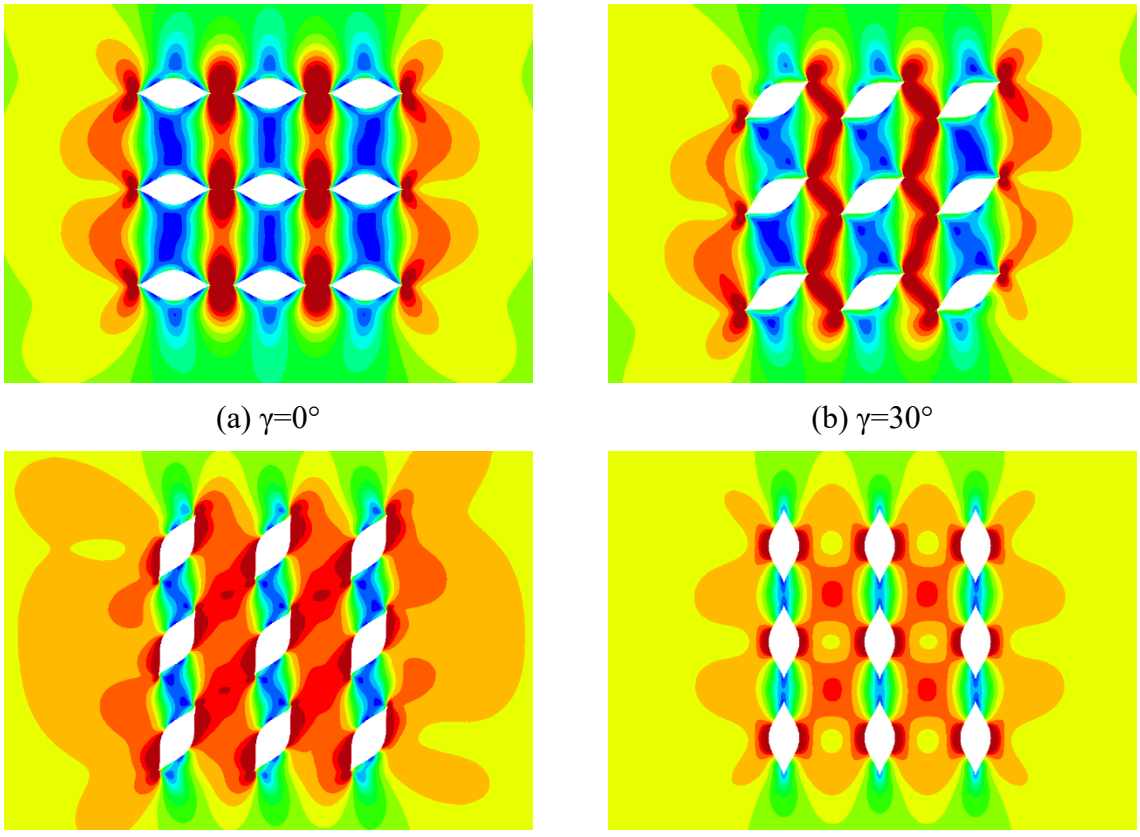

(a) γ=0° (b) γ=30°

(c) γ=60° (d) γ=90°

Figure 7: The stress contours of periodic distribution model at different crack inclination angles.

As shown in Figure 8, in the periodically distributed lip-shaped crack model with an inclination angle of γ=60°, stress concentration was stronger between diagonally adjacent cracks compared to those within the same row, with stress concentration effects remaining consistent across varying width-to-length ratios β. Under these conditions, the crack surfaces were dominated by shear stress, accompanied by a lower energy release rate G, which promotes unstable propagation.

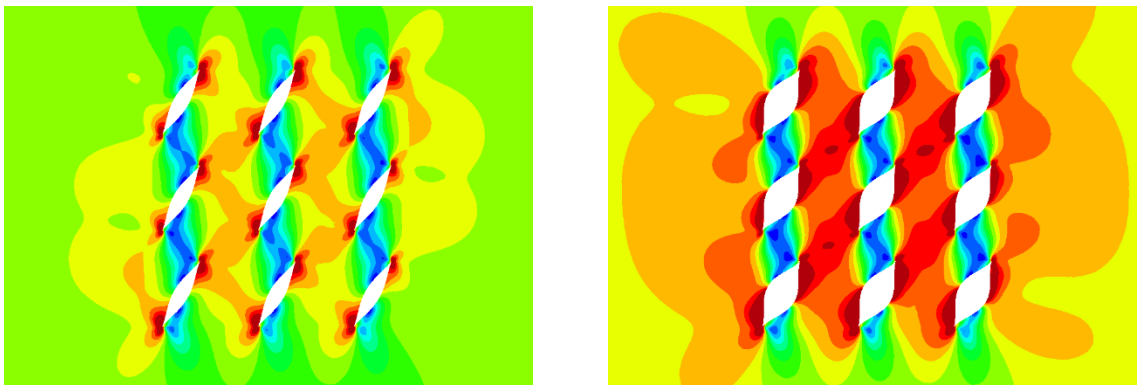

(a) β=0.2 (b) β=0.4

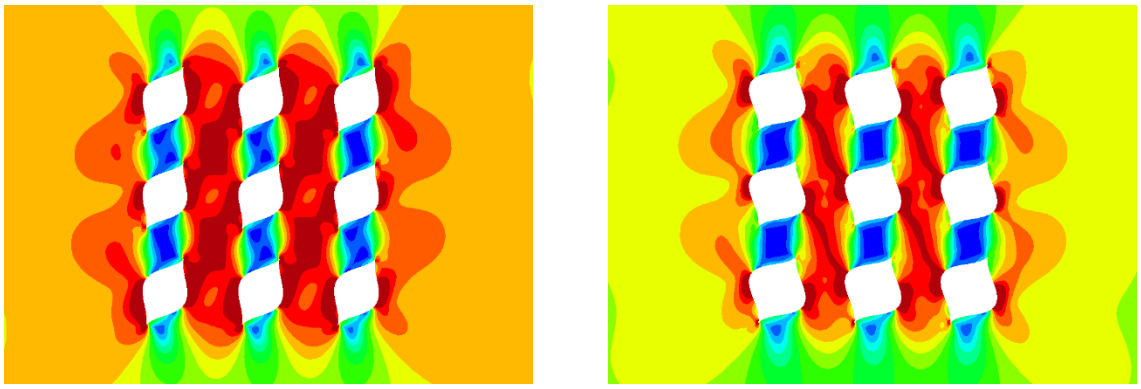

(c) β=0.6 (d) β=0.8

Figure 8: The stress contours of periodic distribution model at different crack width-to-length ratios.

As shown in Figure 9, in the periodically distributed lip-shaped crack model with an inclination angle of γ=30°, closer crack spacing resulted in stronger stress concentration compared to widely spaced situations. However, the crack surface orientations and cracking angles θ_0 remained nearly identical across spacing variations, indicating that crack spacing primarily governs the ease of crack initiation and propagation rather than coalescence patterns.

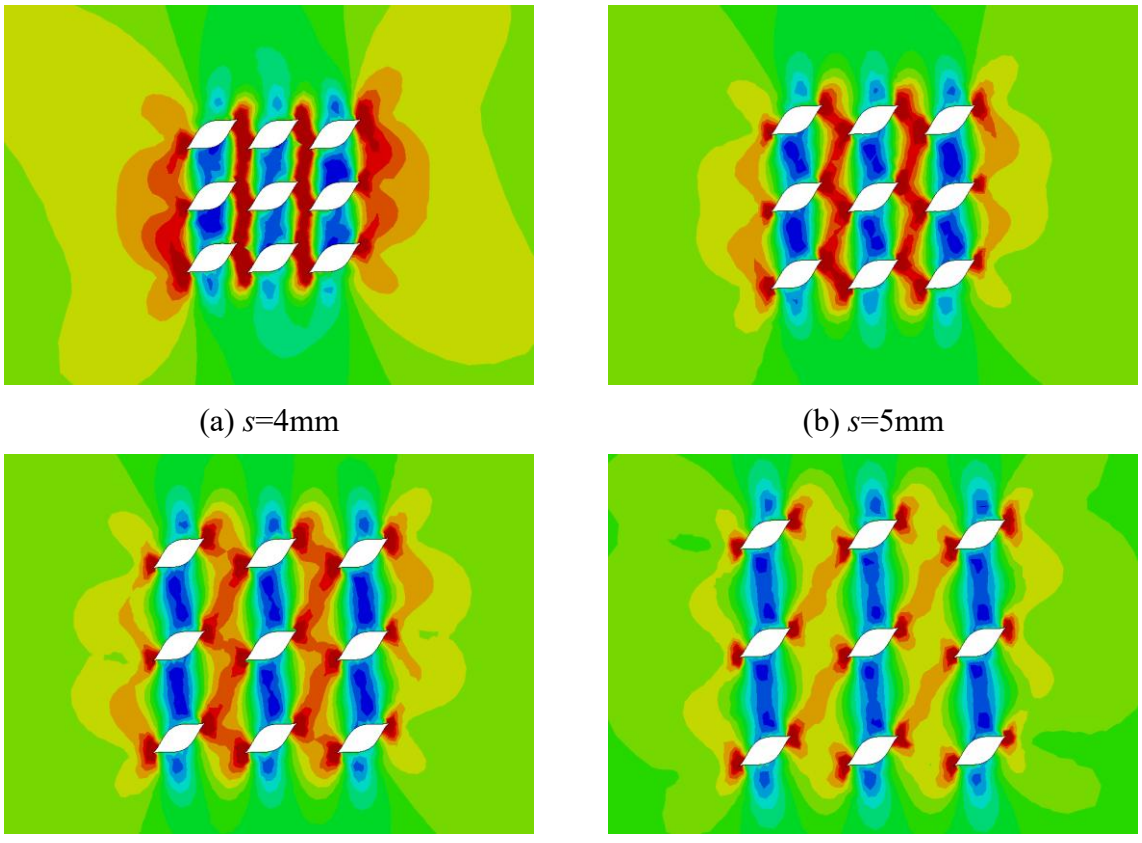

(a) s=4mm (b) s=5mm

(c) s=6mm (d) s=7mm

Figure 9: The stress contours of periodic distribution model at different crack spacings.

Based on the above analyses, four coalescence patterns (**Figure 10**) are predicted for lip-shaped multiple cracks under varying geometric and loading conditions: Type a (non-

coalescence), universally observed when cracks are misaligned or halted by stress shielding from dominant cracks; Type b (coalescence between tips), prevalent at small inclination angles (adjacent same-row cracks) or moderate inclination angles (γ=30°–60°) with small width-to-length ratios (β) and close spacing (diagonally adjacent cracks);Type c(coalescence between tip and abdomen), dominant at moderate inclination angles (γ=30°–60°, adjacent same-row cracks) or large inclination angles with higher β (adjacent same-column cracks); and Type d (coalescence between abdomens), exclusive to large inclination angles (γ=90°, adjacent same-row cracks).

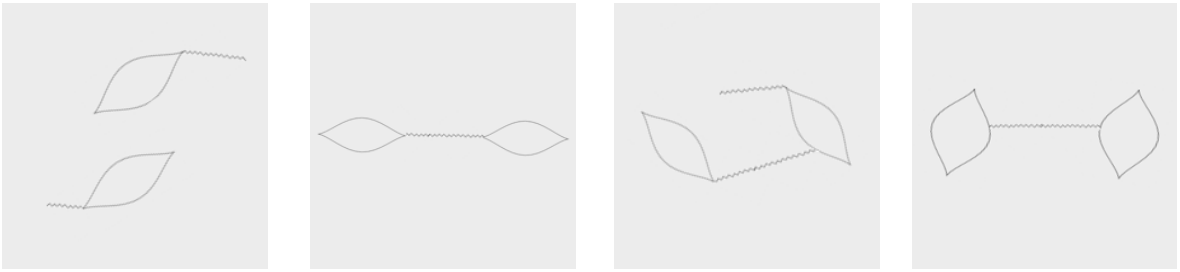

(a) (b) (c) (d)

Figure 10: Schematic diagram of 4 patterns of lip-shaped crack coalescence: (a) No coalescence; (b) Coalescence between tips; (c) Coalescence between tip and abdomen; (d) Coalescence between abdomens

Among these, Type c is likely the most prevalent due to its lower geometric and stress thresholds for initiation. This pattern typically involves crack coalescence from a tip to the abdomen of an adjacent same-row or same-column crack. As shown in Figure 7-a, smaller width-to-length ratios (β) flatten the crack abdomen, increasing the distance to adjacent same-column crack tips and weakening their interaction, thereby favoring same-row Type c coalescence over same-column coalescence.

4 Simulation of Lip-Shaped Multiple Crack Propagation

This section validates the aforementioned coalescence patterns through simulations of crack propagation in periodically distributed lip-shaped multi-crack systems.

4.1 Effect of three factors on crack propagation coalescence

In all model groups, crack initiation predominantly occurred near the crack tips, with subsequent propagation leading to coalescence with adjacent cracks, ultimately forming a macroscopic dominant crack that induced global failure. The first group investigated the influence of crack inclination angle γ (15°, 30°, 45°, 60°, and 75°) on propagation and coalescence, with 25 lip-shaped cracks of width-to-length ratio β=0.4. Crack propagation paths are shown in **Figure 11**.

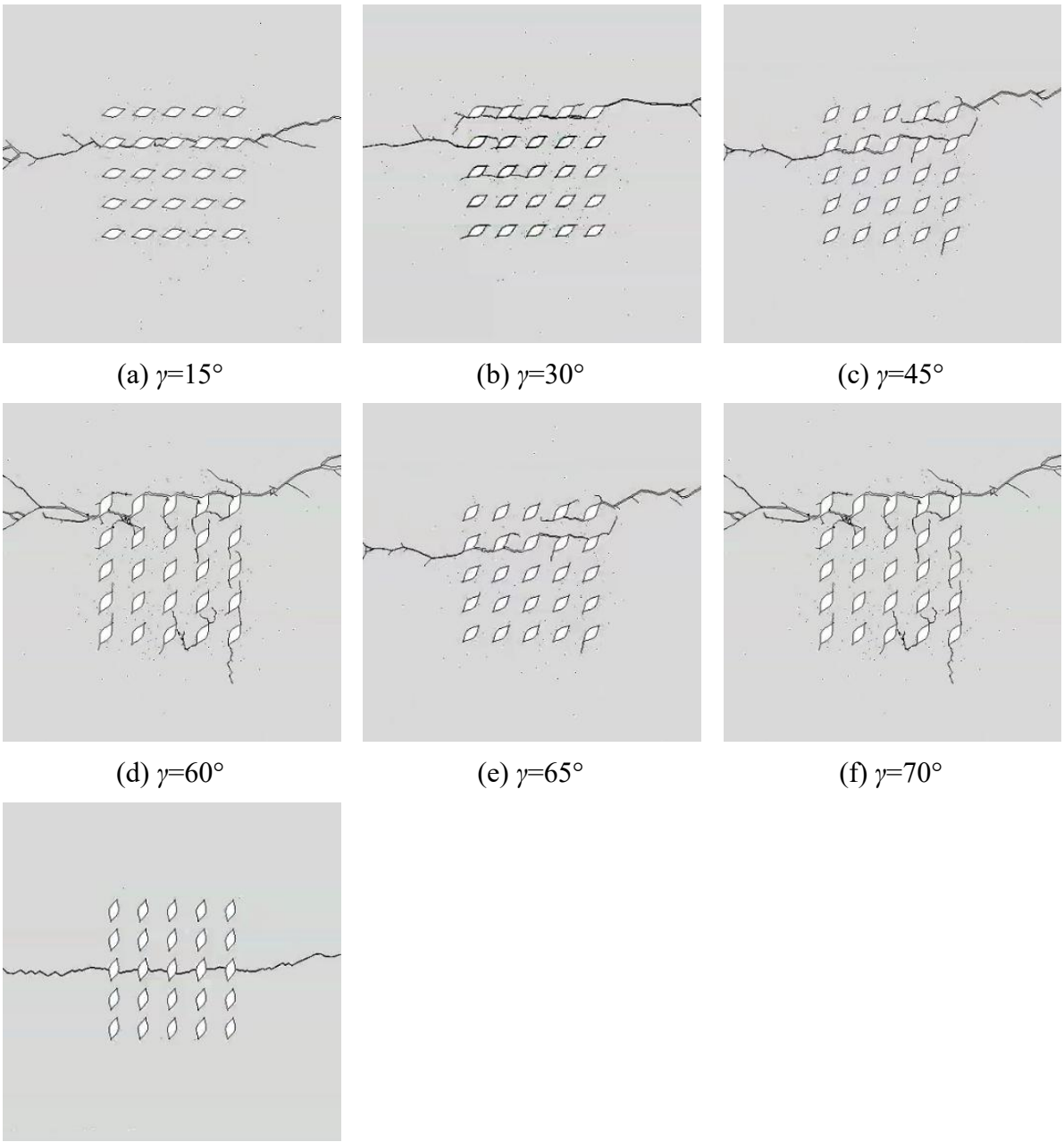

(a) γ=15° (b) γ=30° (c) γ=45°

(d) γ=60° (e) γ=65° (f) γ=70°

(g) γ=75°

Figure 11: Propagation path diagram for different calculation model of different crack inclination angles.

For $\gamma \in [15°,60°]$, cracks initiated at the tips with small cracking angles θ_0, exhibiting near-transverse propagation (perpendicular to the loading direction) dominated by mode I (tensile) fracture. Coalescence primarily involved tip-to-abdomen linkages between adjacent same-row cracks, forming single macroscopic cracks. At γ=60°and 65°, crack initiation directions shifted to near-longitudinal (parallel to loading), demonstrating mode II (shear) dominance, with coalescence patterns transitioning to complex networks involving tip-to-tip and tip-to-abdomen connections across multiple rows. These observations align with Section 2–3 analyses and prior findings [15].

Figure 11(f) reveals concurrent tip and abdomen initiation at higher γ, transitioning to exclusive abdomen-initiated propagation at γ=75°. This shift occurs as stress concentration

migrates from tips to abdomens with increasing γ, reaching a critical transition near γ=70°. Beyond this threshold (e.g., γ=75°), coalescence exclusively involves abdomen-to-abdomen linkages in the same row, confirming the acute sensitivity of coalescence patterns to inclination angle variations.

Additionally, increasing γ significantly reduces the maximum energy release rate G_{max}, promoting unstable propagation with characteristic brittle crack branching (Figure 11). This phenomenon arises from crack-tip field distortion or secondary fracturing during unstable growth [16], consistent with experimental branching patterns, thereby validating the simulation's accuracy.

The second group investigated the effects of varying width-to-length ratios β(0.2, 0.4, 0.6, and 0.8) on crack propagation and coalescence in lip-shaped cracks, with 15 cracks configured at a fixed inclination angle γ=30°. Crack propagation paths are shown in **Figure 12**.

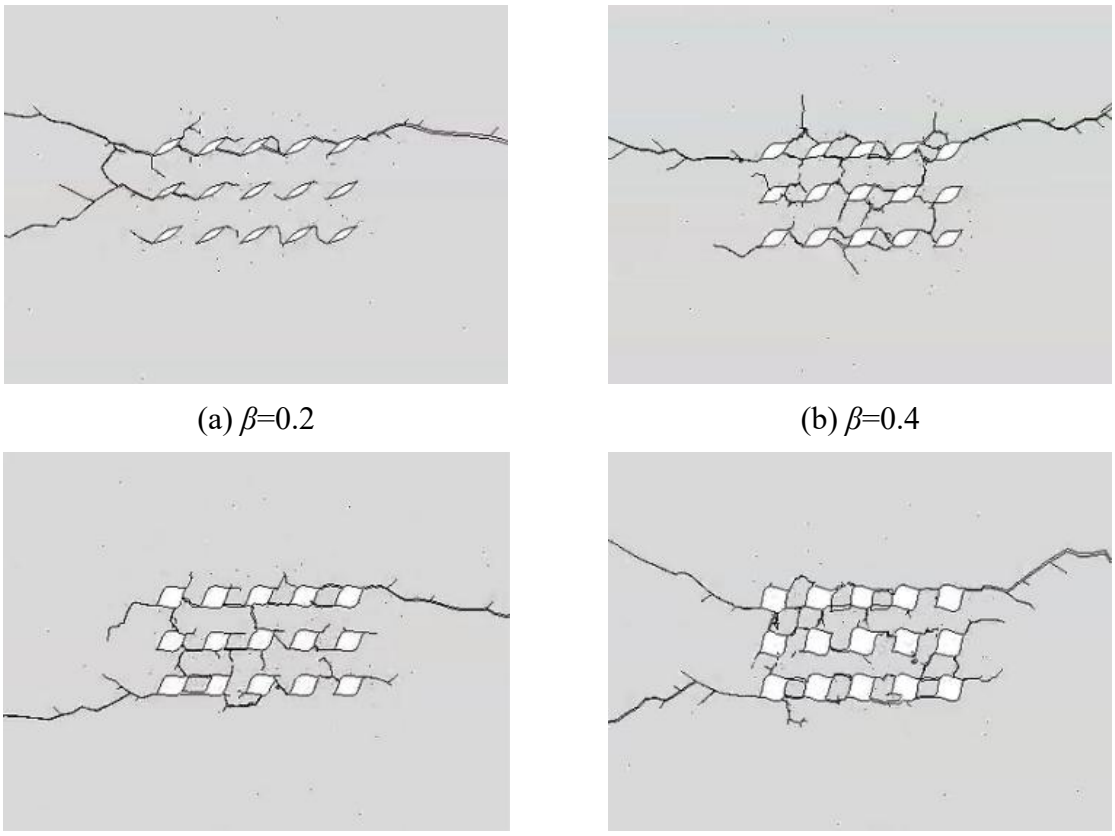

(a) β=0.2 (b) β=0.4

(c) β=0.6 (d) β=0.8

Figure 12: Propagation path diagram for different calculation model of different width-to-length ratios.

Figure 12 shows that in periodically distributed multiple crack models, larger width-to-length ratios β facilitate increased coalescence likelihood, with patterns transitioning from simple tip-to-tip or tip-to-abdomen connections within the same row to complex configurations involving both these modes and additional abdomen-to-tip or abdomen-to-abdomen linkages across adjacent columns. These results align with Section 3 predictions, confirming that higher β values induce more complex coalescence behaviors.

The third group examined the influence of crack spacing s (4 mm, 5 mm, 6 mm, and 7 mm) on coalescence, with lip-shaped cracks configured at γ=30° and β=0.4. Crack propagation paths are illustrated in **Figure 13**.

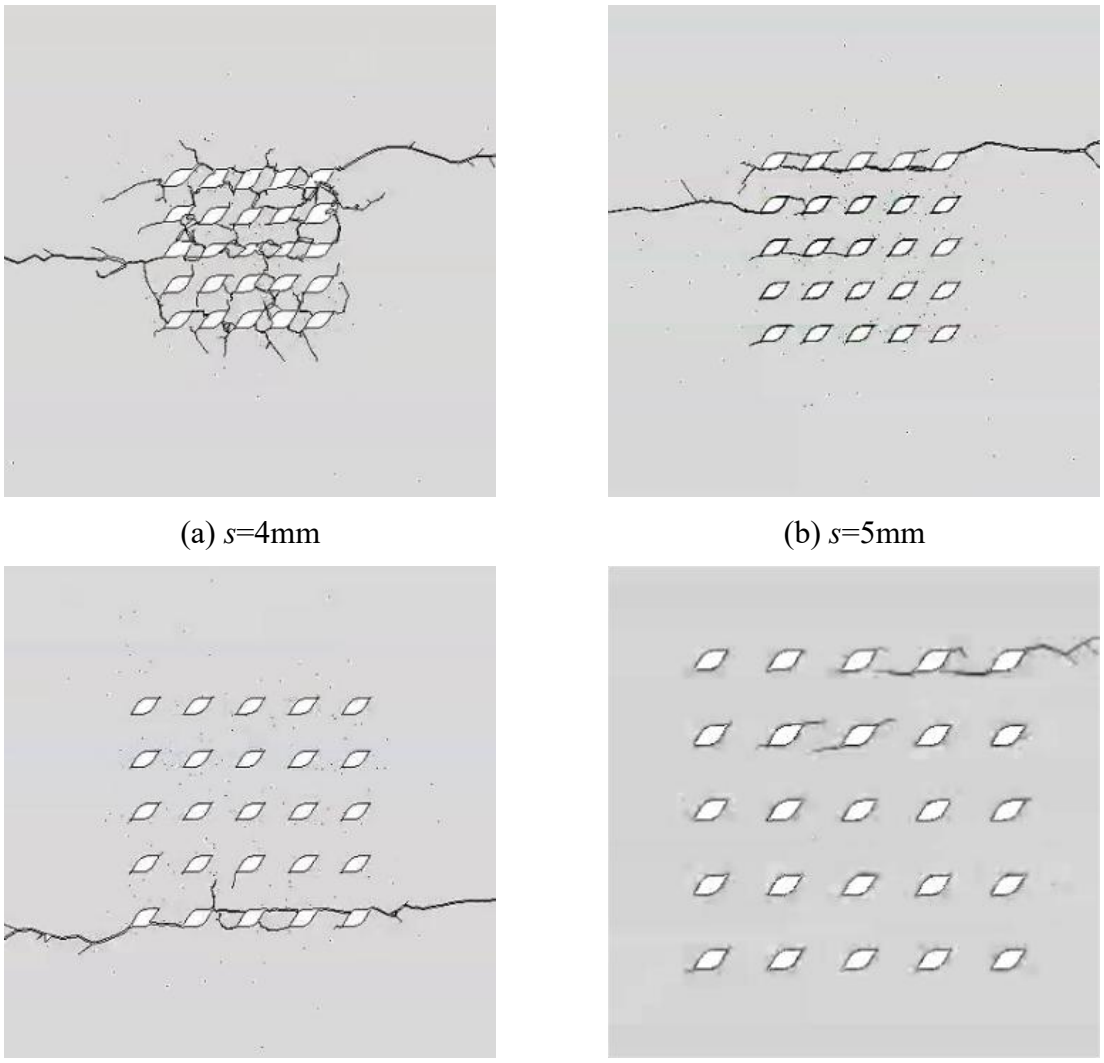

(a) *s*=4mm (b) *s*=5mm

(a) *s*=6mm (b) *s*=7mm

Figure 13: Propagation path diagram for different calculation model of different crack spacings.

Figure 13 demonstrates that coalescence predominantly occurs between tip and abdomen across all crack spacing *s*. Under identical loading conditions, models with smaller *s* exhibit more frequent crack initiation and coalescence compared to widely spaced situations, aligning with Section 3 findings and the consensus that closer cracks accelerate failure. This confirms that spacing minimally affects coalescence patterns but governs failure susceptibility: reduce *s* intensifies stress concentration at crack tips, enabling the crack-tip energy release rate to reach its maximum faster and promoting earlier failure.

Overall, simulated coalescence patterns and their triggering conditions broadly match previous predictions.

Figure 14 presents fracture and propagation paths from experiment in literature [16, 17]. Figure 14(a) displays specimen coalescence under SHPB test, where coalescence occurs via crack propagation from a tip to another crack tip, analogous to the Type b coalescence in Figure 10(b). Figure 14(b) shows crack paths from tensile tests on PMMA plates with pre-existing parallel cracks by Reference [17], where coalescence occurs via crack propagation from a tip to another crack's abdomen, analogous to the Type c coalescence in Figure 10(c). Both cases align with the predictions.

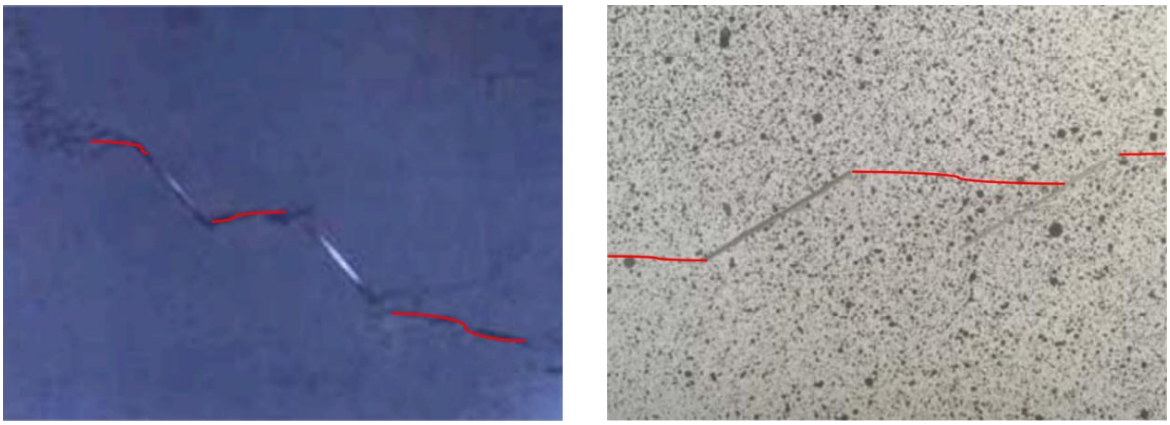

(a) (b)

Figure 14: Diagram of typical fracture feature and crack propagation path from experiment: (a) Schematic of specimen coalescence under SHPB test; (b) Crack propagation path diagram obtained from experiment

Figure 15 is the crack propagation path diagram obtained by simulating two situations similar to figure 14, which is almost consistent with the path in figure 14, validating the proposed model's accuracy.

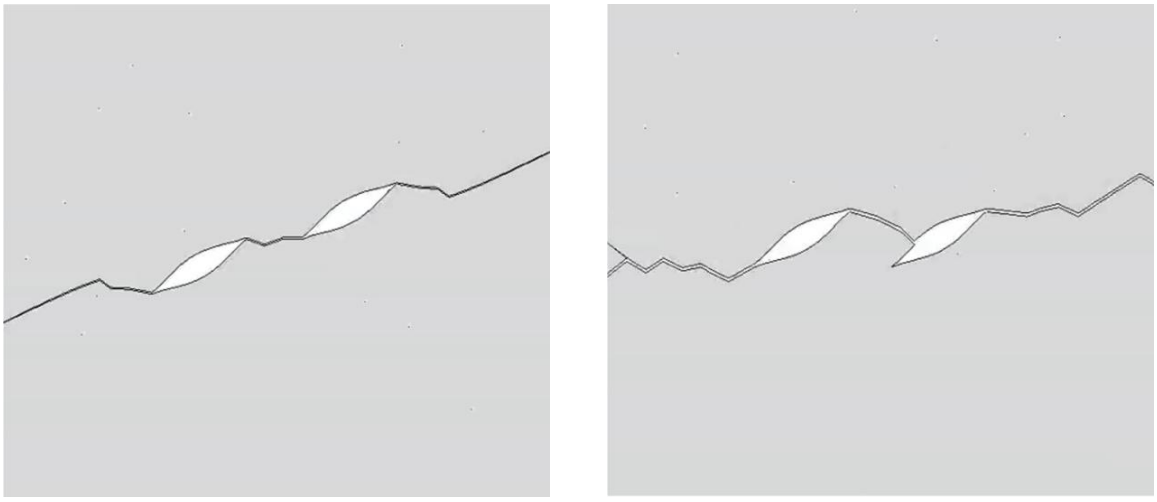

(a) (b)

Figure 15: Diagram of simulations similar to figure 13: (a) simulation similar to figure 13(a); (b) simulation similar to figure 13(b)

4.2 Effect of three factors on constitutive relations

The stress-strain curves corresponding to these three model groups are shown in Figures 16, 17, and 18. As seen in **Figure 16** (stress-strain curves for varying crack inclination angles), the overall stiffness and tensile strength of the model increase with increasing inclination angle. The tensile strength and stiffness at 15° and 30° is nearly identical, the strengths at 45°, 60°, and 75° are enhanced by approximately 22.9%, 44.1%, and 48.4%, respectively, the stiffness increases by approximately 8.7%, 14.5%, and 18.2% respectively, compared to the 15° case. This indicates that model tensile strength stiffness progressively rise with inclination angle.

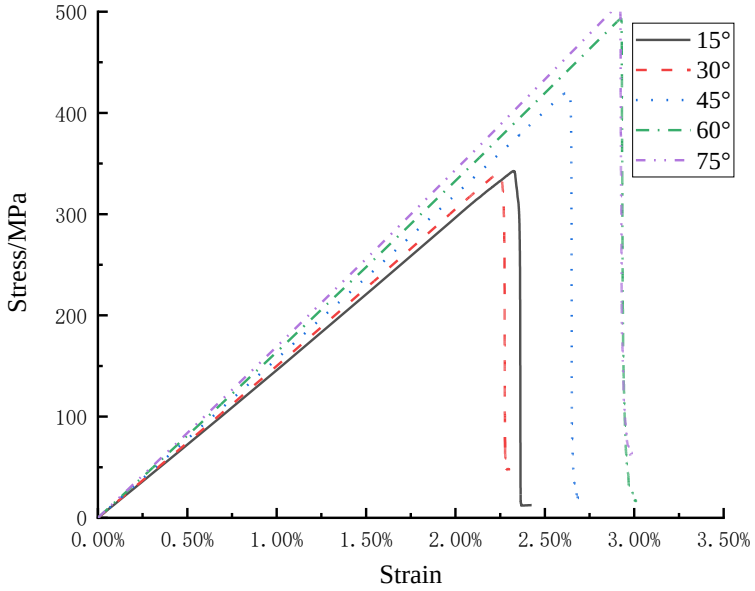

Figure 16: Model stress-strain curves of different crack inclination angles

The stress-strain curves for models with varying width-to-length ratios β are shown in **Figure 17**. The results indicate negligible differences in tensile strength and stiffness across different β values in periodically distributed lip-shaped crack systems, confirming that the width-to-length ratio has rarely impact on model performance.

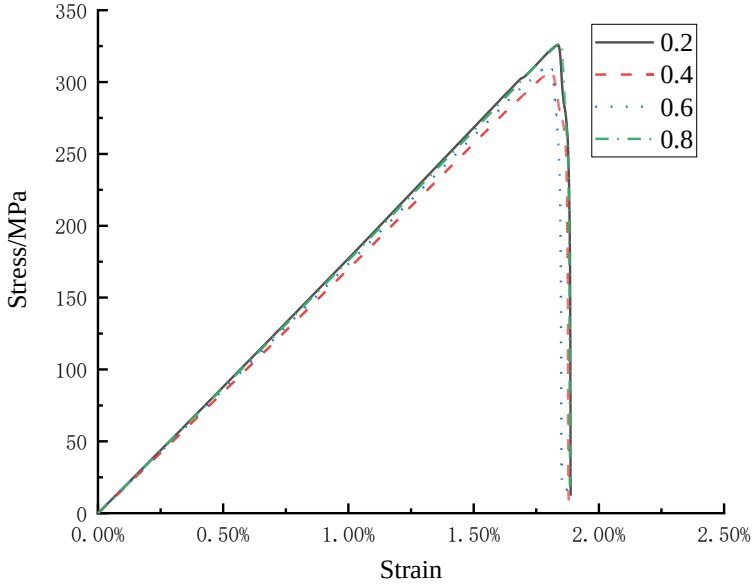

Figure 17: Model stress-strain curves of different width-to-length ratios β

The model stress and strain curves under different crack spacings are shown in **Figure 18**. As the crack spacing decreases, the failure displacement of periodically distributed lip-shaped crack model is decreased. In the periodic model of 25 lip-shaped cracks with inclination angle of 30° and width-to-length ratio of 0.4, compared with the failure displacement of 7mm spacing model, reducing the crack spacing made the model's failure displacement decreased by 11.4% (6mm), 18.1% (5mm), and 21.8% (4mm), respectively. The tensile strength was reduced by only 3.9% (6mm), 3.3% (5mm), and 0.8% (4mm), respectively, which shows that the crack

spacing has a significant impact on the model failure displacement, but has almost no effect on the tensile strength.

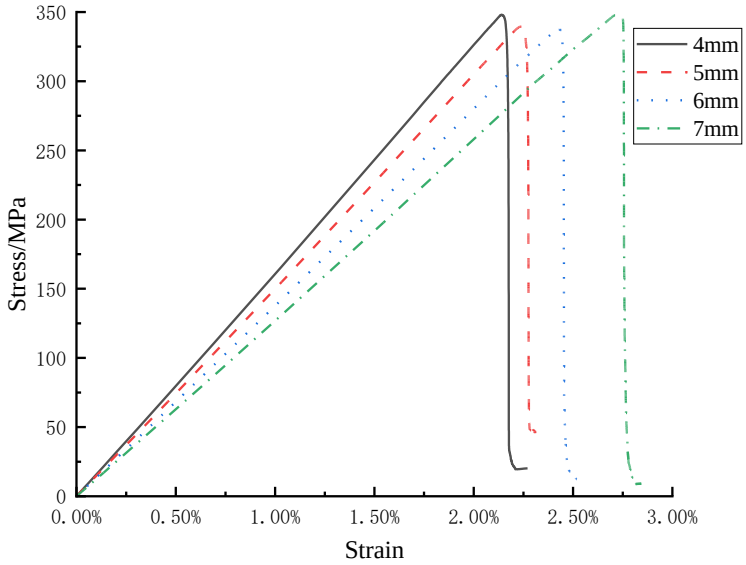

Figure 18: Model stress-strain curves of different crack spacings s

The tensile strength σ_f, stiffness K_s and failure displacement d_f of the stress-strain curves corresponding to the above models of γ and s are shown in **Table 3**.

Table 3: The tensile strength σ_f, stiffness K_s and failure displacement d_f corresponding to the above models of γ and s

Items	Failure Displacement d_f/(mm)	Tensile Strength σ_f/(MPa)	Stiffness K_s/(MPa mm^{-1})	Change Magnitude of d_f	Change Magnitude of σ_f	Change Magnitude of K_s
γ=15°	2.326	342.597	147.29	Δ[1]		
γ=45°	2.629	421.089	160.17	13.0%	22.9%	8.7%
γ=60°	2.926	493.562	168.68	25.8%	44.1%	14.5%
γ=75°	2.92	508.449	174.13	25.5%	48.4%	18.2%
s=4mm	2.14	348.081	162.65	21.8%	0.8%	26.8%
s=5mm	2.239	339.49	151.63	18.1%	3.3%	18.2%
s=6mm	2.424	337.43	139.20	11.4%	3.9%	8.5%
s=7mm	2.735	350.954	128.32	Δ		

[1] Δ means the item being compared.

5 Conclusion

In this study, a mathematical model of lip-shaped crack established through complex variable function and angle-conservative mapping, then lip-shaped crack tip failure criterion under uniaxial tensile load based on the energy release rate criterion established; for different crack inclination angles, width-length ratios and crack spacings, three numerical calculation models with periodic distribution of lip-shaped cracks were established, and the coalescence rules of lip-shaped cracks in brittle materials were discussed, and the following conclusions were obtained:

1) Four coalescence patterns of lip-shaped multiple cracks were summarized, thereinto the most common coalescence pattern is the coalescence between tip and abdomen. The coalescence pattern is most sensitive to the change of crack inclination angle;

2) Compared with the experimental results, this study successfully simulates the complex coalescences in brittle materials: the macroscopic main crack is mainly formed by the composite and cross of the four basic coalescence patterns, and the bifurcation reflects the instability state of the model as it fails;

3) The crack inclination angle and spacing of lip-shaped cracks have a significant impact on the performance of the model: the smaller the crack inclination angle, the smaller the tensile strength and the greater the stiffness of the model; the smaller the crack spacing, the smaller the model failure displacement.

Author Contributions

Conceptualization, X.L. and X.H.; methodology, T.L.; software, T.L. and Y.F.; validation, T.L., H.Z. and Y.F.; formal analysis, T.L. and Y.F.; investigation, T.L.; resources, X.L.; data curation, X.L.; writing—original draft preparation, T.L.; writing—review and editing, T.L. and Y.F.; visualization, T.L. and Y.F..; supervision, X.H. and H.Z.; project administration, H.Z.; funding acquisition, H.Z. All authors have read and agreed to the published version of the manuscript.

Funding

This study was funded by Fundamental Research Funds for Central Universities, grant number 3122022098. In addition, the authors would like to express great appreciation to the reviewers for their valuable comments and suggestions that helped improve the quality of the paper.

Institutional Review Board Statement

Not applicable.

Informed Consent Statement

Not applicable.

Data Availability Statement

The raw data supporting the conclusions of this article will be made available by the authors on request.

Conflicts of Interest

The authors declare no conflicts of interest.

Abbreviations

The following abbreviations are used in this manuscript:

SIF	Stress Intensity Factor
MERR	Maximum Energy Release Rate
LEFM	Linear Elastic Fracture Mechanics
PMMA	Polymethyl Methacrylate

About The Author

Tianzhu Liu was born in Suizhou, Hubei.P.R. China, in 2001. He obtained a bachelor's degree from Civil Aviation University of China. I am currently studying at the Sino-European Institute of Aviation Engineering, Civil Aviation University of China. My main research direction is Aircraft structure and material. 2022122021@cauc.edu.cn

References

[1] Belabed Z, Tounsi A, Bousahla A A, et al. Mechanical behavior analysis of FG-CNTRC porous beams resting on Winkler and Pasternak elastic foundations: a finite element approach[J]. Computers and Concrete, 2024, 34(4): 447-465.

[2] Ito C, Maeda T, Higashi R, et al. Application of extreme value statistics to internal pore distribution in ceramics and prediction of size dependency of strength scatter[J]. Journal of the European Ceramic Society, 2024, 44(5): 3381-3392.

[3] Rozen-Levy L, Kolinski J M, Cohen G, et al. How fast cracks in brittle solids choose their path[J]. Physical review letters, 2020, 125(17): 175501.

[4] Kiyani E, Manav M, Kadivar N, et al. Predicting crack nucleation and propagation in brittle materials using deep operator networks with diverse trunk architectures[J]. Computer Methods in Applied Mechanics and Engineering, 2025, 441: 117984.

[5] Mohammadi S, Torabi A R. A review on ductile fracture prediction of cracked/notched components: The distinct and simplifying roles of the equivalent material concept and fictitious material concept[J]. Theoretical and Applied Fracture Mechanics, 2024, 130: 104290.

[6] Wang M, Bouchbinder E, Fineberg J. Size Selection of Crack Front Defects: Multiple Fracture-Plane Interactions and Intrinsic Length Scales[J]. Physical Review Letters, 2024, 133(15): 156201.

[7] Altay U, Dorduncu M, Kadioglu S. Dual horizon peridynamic approach for studying the effect of porous media on the dynamic crack growth in brittle materials[J]. Journal of Peridynamics and Nonlocal Modeling, 2024, 6(3): 505-529.

[8] Dudyk M, Kaminsky A, Reshitnyk Y, et al. On analytical model of interface crack in bonding quasi-brittle material between distinct elastic media[J]. Procedia Structural Integrity, 2025, 68: 53-58.

[9] Kanaya T, Hirth G. Role of crack interaction on shear localization in porous granular rocks deformed in the brittle and ductile fields[J]. Journal of Geophysical Research: Solid Earth, 2024, 129(4): e2023JB027316.

[10] Eghbalpoor R, Sheidaei A. A peridynamic-informed deep learning model for brittle damage prediction[J]. Theoretical and Applied Fracture Mechanics, 2024, 131: 104457.

[11] Shichalin O O, Ivanov N P, Seroshtan A I, et al. Spark plasma sintering of Ti2AlC/TiC MAX-phase based composite ceramic materials and study of their electrochemical characteristics[J]. Ceramics International, 2024, 50(24): 53120-53128.

[12] Niziołek K, Słota D, Sobczak-Kupiec A. Polysaccharide-based composite systems in bone tissue engineering: a review[J]. Materials, 2024, 17(17): 4220.

[13] Shen QQ, Rao QH, Li Z, et al. Interacting mechanism and initiation prediction of multiple cracks. Trans Nonferrous Met Soc China. 2021;31(3):779-791.

[14] Al-Hasani F J, Hamad Q A, Faheed N K. Enhancing the cell viability and antibacterial properties of alginate-based composite layer by adding active particulates[J]. Discover Applied Sciences, 2024, 6(2): 70-86.

[15] Sharma S K, Gajević S, Sharma L K, et al. Progress in aluminum-based composites prepared by stir casting: mechanical and tribological properties for automotive, aerospace, and military applications[J]. Lubricants, 2024, 12(12): 421-437.

[16] Agarwal N, Rangamani A, Bhavsar K, et al. An overview of carbon-carbon composite materials and their applications[J]. Frontiers in Materials, 2024, 11: 1374034.

[17] Singh S, Bhaskar R, Narayanan K B, et al. Development of silicon carbide (SiC)-based composites as microwave-absorbing materials (MAMs): A review[J]. Journal of the European Ceramic Society, 2024, 44(13): 7411-7431.